Goran Kovačević, Luc Nicoleau, André Nonat, and
Valera Veryazov*

Revised Atomistic Models of the Crystal Structure of C–S–H with high C/S Ratio

DOI 10.1515/zpch-2015-0718
Received October 20, 2015; accepted April 9, 2016

Abstract: The atomic structure of calcium-silicate-hydrate ($C_{1.67}$–S–H_x) has been studied. Atomistic C–S–H models suggested in our previous study have been revised in order to perform a direct comparison of energetic stability of the different structures. An extensive set of periodic structures of C–S–H with variation of water content was created, and then optimized using molecular dynamics with reactive force field ReaxFF and quantum chemical semiempirical method PM6. All models show organization of water molecules inside the structure of C–S–H. The new geometries of C–S–H, reported in this paper, show lower relative energy with respect to the geometries from the original definition of C–S–H models. Model that corresponds to calcium enriched tobermorite structure has the lowest relative energy and the density closest to the experimental values.

Keywords: C–S–H Structure, Atomistic Simulation, ReaxFF Force Field, Semiempirical Quantum Chemistry.

1 Introduction

The atomic structure of Calcium-Silicate-Hydrate (C–S–H) has many uncertainties, despite being a subject of research for a long time [1–4]. The structure is determined to be similar to the layered structure of a natural calcium silicate hydrate: tobermorite [4–8]. Each layer consists of arrays of positive calcium ions, sandwiched with negative silica chains. The space between layers is filled with calcium

***Corresponding author: Valera Veryazov,** Lund University, Lund, Sweden,
e-mail: valera.veryazov@teokem.lu.se
Goran Kovačević: Ruđer Bošković Institute, Zagreb, Croatia; and Lund University, Lund, Sweden
Luc Nicoleau: BASF Construction Materials & Systems Research, Trostberg, Germany
André Nonat: CNRS-Université de Bourgogne-Franche Comté, Dijon, France

ions and with water molecules. Several atomic models based on the tobermorite layered structure has been proposed [4, 6, 9–12].

The detailed knowledge of C–S–H structure on atomic level is essential for the understanding physical properties and chemical bonding of C–S–H materials. Without a detailed description of C–S–H structure and information about the exact position of atoms it is impossible to make non empirical theoretical modelling of C–S–H particles and their surfaces. In the same time, concrete-like materials demonstrate the absence of regular crystal structure and thus the problem of finding atomic structure (or structures) of C–S–H becomes uneasy and probably unresolvable task.

^{29}Si NMR studies [2, 4] have shown that in pure C–S–H at high C/S, bridging tertiary silica groups (Q_3) do not exist. ^{29}Si NMR studies also found no conclusive evidence about the existence of monomeric (Q_0) silica units. The ratio Q_2/Q_1 is determined to be about 0.2 [5, 13, 14].

Crystal phases are usually represented by an unit cell. Unfortunately, C–S–H structure lacks long range crystal order and, therefore representation by the single unit cell is too crude approximation. We solved the problem [15] of representing the structure of C–S–H by using multitude of unit cells, each with different statistical distribution of silica dimers and pentamers. Each structure, belonging to the same model obeys to the certain crystallographic principles. Properties of C–S–H can be obtained as the average value of properties from each geometry. There are many ways to select crystallographic rules for building structures that can reproduce known amount of calcium atoms and ratio of silicon atoms in Q1 and Q2 positions [5, 13, 14]. Based on sparse experimental knowledge about C–S–H structure, we proposed [15] three distinctive crystallographic models, that differ in the statistical distribution of oligomeric silica units and the location of calcium ions. Within each crystallographic model, we created a large number of structures in order to determine relative stability of models in terms of energy and their density that can be related to experimental results. All models were created from the tobermorite 11 Å structure [16]. A chemical composition of tobermorite is, however, different from one in C–S–H phase and there are several ways to adjust it: either by enriching the structure by extra calcium atoms, or by removing the excess of silicon. The amount of hydrogen, in the form of either water or hydroxyl groups, also should be adjusted.

Model 1 corresponds to calcium enriched tobermorite structure with partially removed silica tetrahedrons. Model 2 is based on tobermorite structure with jennite like defects. In both models the removal of an excess of SiO_2 is performed in a controlled way, thus silica monomers cannot appear. In model 3, in contrary, a randomly removed SiO_2 fragments may lead to the formation of silica monomers. The construction of the actual structures for these models is described

in details in [15]. An inbuilt property for all these models is a random character of created defects. Thus, each model is represented by a wide set of crystal structures which obey to the certain crystallographic principles. In the first part of our paper, our main objective was the construction of the structures which describe these three crystallographic models. The actual composition of constructed unit cells could vary both inside a model and in between models. These variations in the composition complicate the direct comparison of the models, and any conclusion about more stable configuration requires additional assumptions, for example, a scaling procedure should be implemented. Also, these models differ in the amount of protonation of silica units, which leads to unequal H/S ratio. Since the composition of C–S–H ($Ca_xSi_yH_zO_{x+2y+z/2}$) contains two independent parameters, the comparison between different geometries require additional assumptions and can not be performed directly.

Therefore, in the current study we have modified the algorithms used in [15], and applied additional condition, so all structures have an identical chemical composition per unit cell (both inside one model and across different models). The atomic composition of an unit cell of each structure is identical, thus the total energies can be compared directly, without any additional approximations and assumptions. The previous results for obtained for the structures in [15] we will refer in the paper as $1^{\dagger}$, $2^{\dagger}$ and $3^{\dagger}$.

Within our approach, the crystallographic information about the structure of C–S–H plays the major role, and we consider the following structure optimization (using molecular dynamics with a force field and semiempirical quantum chemical simulations) only as a method to relax the proposed structures and keeping the main characteristics of Si and Ca networks. An alternative approach [12, 17, 18] involving long time molecular dynamic simulation is, at least theoretically, a better strategy to find more stable structure for C–S–H. However, the reorganization of the Si–O network involves very high energy barriers, and in order to pass through this transition, a large temperature should be applied to the system. In addition to that, the structures obtained in large scale/high temperature MD simulations with distorted Si–O skeleton are more difficult to classify.

2 The construction of geometrical models

2.1 Crystallographic models of C–S–H

The geometries belonging to models 1–3 are constructed from the same initial structure of tobermorite 11 Å suggested at [16]. Redefined model 1 is created fol-

TS[a] Please check and confirm the short running title.

Editor's or typesetter's annotations (will be removed before the final TEX run)

Table 1: Unit cell sizes of models 1, 2 and 3. Unit cells are not optimized. α and γ angles are 90.0°.

	model 1	model 2	model 3
a/Å	29.48	36.84	36.84
b/Å	20.95	19.90	19.90
c/Å	22.78	22.68	22.68
β/deg	58.17	58.17	58.17

lowing the same way as model $1^{\dagger}$: by fragmenting infinite silica chains of tobermorite by randomly removing silica monomers from Si2 sites (generally referred to bridging tetrahedrons) and adjusting the expected C/S ratio (1.67) by adding Ca atoms into the interlayer. Since model $1^{\dagger}$ had 17% more atoms than models $2^{\dagger}$ and $3^{\dagger}$, model 1 is created smaller than model $1^{\dagger}$ in order to have the same number of atoms as models 2 and 3.

Initial unit cells of models 1 were created as a $3\times4\times1$ supercell of tobermorite 11 Å (see Table 1).

Model 2 is created with the same basic idea as for model $2^{\dagger}$: removing four consecutive silica atoms from the infinite silica chains of tobermorite. These four consecutive silica atoms are always Si2-Si1-Si3-Si2 positions and the position of the chain is selected randomly in order to create the distribution of silica dimers and pentamers. 22 calcium atoms have to be removed from the structure in order to make the correct C/S ratio and to make the structures with the same number of atoms as in structures of model 1. Unit cells of model 2 are $3 \times 5 \times 1$ supercells of tobermorite. Unlike model $2^{\dagger}$, where silica units were heavily protonated, in model 2 silica units were left without hydrogen atoms.

Model 3 is created in a similar fashion as model $3^{\dagger}$: with random removal of silicon atoms, no matter on the site of the removed atom. The ratio of silica units in Q_1 and Q_2 sites in oligomers, created by random removal of silica units from infinite silica chains, does not match experimentally observed Q_1/Q_2 ratio. Also, random removal of silica units produces about 36% silica monomers, which is by far greater than experimentally observed amount in samples that are possibly contaminated with the C_3S phase. Therefore, we discarded all structures with less than 12% of Si(Q_0) atoms, more than 86% Si(Q_1) atoms or more than 14% Si(Q_2) atoms. This makes the process of creation of model 3 structures very inefficient, since only a small fraction satisfied these conditions, but the resulting structures have Q_1/Q_2 ratio close to experimental one. The unit cells of model 3 are also $3 \times 5 \times 1$ supercells of tobermorite. As in model 1, silica units were not protonated. Unlike models $1^{\dagger}$–$3^{\dagger}$, where silica units were heavily protonated, in

Table 2: Distribution of oligomers in different C–S–H models. Models $1^{\dagger}$–$3^{\dagger}$ are from [15], models 1–3 – the current study. Oligomer size shows the number of silicon atoms in a chain.

Oligomer size	model $1^{\dagger}$	model 1	model $2^{\dagger}$	model 2	model $3^{\dagger}$	model 3
1	0	0	0	0	27.4%	10.2%
2	86.9%	72.0%	84.6%	71.8%	38.2%	49.7%
3	0	0	0	0	12.0%	17.9%
4	0	0	0	0	8.8%	11.2%
5	12.0%	22.8%	13.3%	23.6%	7.4%	7.3%
6	0	0	0	0	1.9%	2.2%
7	0	0	0	0	1.5%	0.8%
8	1.0%	4.6%	1.9%	4.1%	1.1%	0.3%
9	0	0	0	0	0.5%	0.1%
1	0	0	0	0	0.3%	0.02%
11	0.07%	0.6%	0.2%	0.5%	0.6%	0
> 11	0	0.03%	0	0.03%	0.04%	0

models 1–3 silica units were left without hydrogen atoms in agreement with titration experiments [19].

For comparison, the distribution of oligomers in all models is shown in Table 2.

Another difference in building modified models 1–3 with respect to the original models $1^{\dagger}$–$3^{\dagger}$ is in placing water molecules. In models $1^{\dagger}$–$3^{\dagger}$ positions of water molecules are taken from crystallographic data of tobermorite 11 Å [16] and shifted if necessary in order to avoid close contacts. In case of models 1, 2, 3, all water molecules were removed before starting procedures of modifying silica chains. The next step is removal of silica in order to produce oligomers. Since calcium atoms in intralayer are coordinated with oxygen atoms from silica oligomers, calcium atoms are removed only from the interlayer. After that, oxygen atoms that are left uncoordinated are removed. At this moment basic skeleton of calcium atoms and silica groups is finished and all geometries in all models have the same number of silicon and calcium atoms. The next step consists of adding water molecules to the finished skeletons. The number of water molecules that are added depends on the desired H/S ratio. The water molecules are added with Packmol software [20]. Packmol optimizes position of water molecules using the box-constrained minimization algorithm (BOX-QUACAN) [21]. This method has the advantage over using crystallographic positions of water. Some crystal positions in tobermorite 11 Å structure have partial occupancy and in models 1–3 a full occupancy of calcium atoms is assigned. Also in model 1 interlayer calcium positions are doubled. That created multiple steric problems that had to

Table 3: H/S ratios used in building models 1, 2, 3 and their corresponding chemical compositions.

H/S ratio	composition per unit cell
1.4	$Si_{102}Ca_{170}O_{517}H_{286}$
1.6	$Si_{102}Ca_{170}O_{532}H_{326}$
1.8	$Si_{102}Ca_{170}O_{557}H_{366}$
2.0	$Si_{102}Ca_{170}O_{578}H_{408}$

be solved with adjusting positions of water molecules and even with expanding unit cells. In models 1, 2 and 3, by using box-constrained optimization, water molecules are added evenly and filled every void in the structure. This algorithm has its downsides since it does treat water molecules as hard geometrical objects and it does not respect preference of water molecules to create directed hydrogen bonds with other atoms, however geometries with right relative orientations of water molecules are obtained with geometry optimization and molecular dynamics (MD). Box-constrained algorithm, however, makes very good initial geometry for geometry optimization and MD, since it makes geometries without unwanted close contacts that could cause unwanted chemical bonds or extremely large short range repulsion interactions.

Geometries with added water molecules are corrected for charge by removing hydrogen atoms from the added water molecules. Hydrogen atoms that are removed were the atoms that were closest to calcium atoms. In that way negative OH^- groups are created just next to positive calcium atoms which leads to more balanced initial distribution of the point charges. After this correction, all geometries with the same H/S have the same chemical composition (see Table 3). We chose four different H/S ratios and prepared at least ten geometries from each model and each H/S ratios.

At Figure 1 we presented a cartoon explaining the steps taken to construct the models from the basic tobermorite structure. Optional step A corresponds to adding extra Ca atoms. Si tetraherda are removed during step B. And finally water is added in step C.

2.2 Simulation details

Initial optimization and molecular dynamics calculations were done with the LAMMPS program package [22] using the ReaxFF force field [23]. Parametrization of the force field for Si–O–H and Ca–O–H systems was suggested at [24, 25]. In

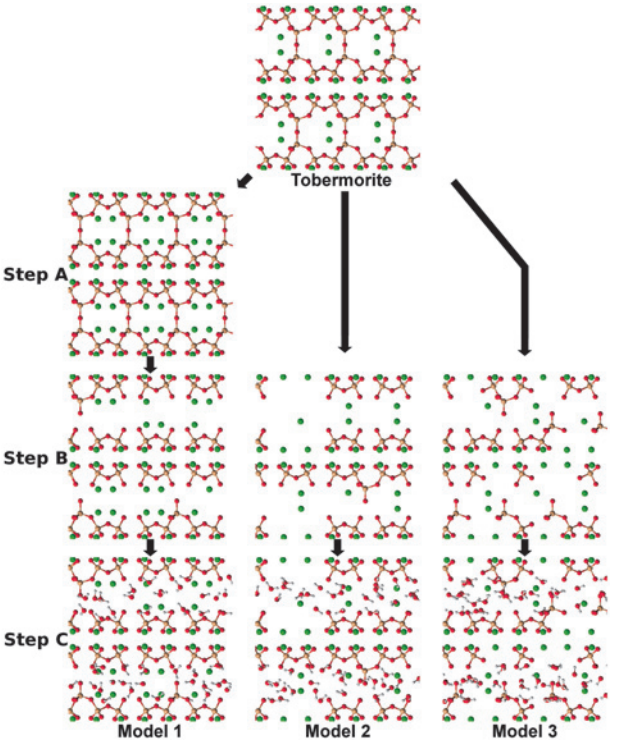

Figure 1: Sample of unit cells of models 1 (a), 2 (b), 3 (c). Unit cells are shown without water molecules for clarity. TS[b]

our study, a modified $\text{ReaxFF}_{\text{SiO:CaO}}$ parameter set was used, in order to describe oxygen atoms in silica and in water. In the parameter set used for oxygen atoms in silica groups, covalent bonding with hydrogen atoms is disabled in order to prevent proton transfer from water molecules to silica units during MD simulations to keep, according to experiments, silicates deprotonated. The ability of these atoms to make hydrogen bonds is retained in this parameter set.

Calculations are performed in several steps in order to preserve, if possible, Si–O skeleton:

1. geometry optimization of atoms in interlayer. Atoms in intralayer are frozen.
2. MD, 5 ps, temperature is ramped from 0.1 K to 500 K, atoms in intralayer are frozen.
3. geometry optimization without frozen atoms.
4. MD, 1 ps, 0.1 K
5. geometry optimization
6. MD, 5 ps, temperature is razed to 300 K
7. geometry optimization
8. geometries from steps 5 and 7 were reoptimized with the $\text{ReaxFF}_{\text{SiO:CaO}}$

TS[b] Please check if correct figure and caption are used.

Editor's or typesetter's annotations (will be removed before the final TEX run)

The first step is the optimization of water molecules and calcium ions in the interlayer, while all atoms in the intralayer are left frozen. This step is important since box-constrained minimization algorithm left water molecules that were not ideally oriented and hydrogen bonds are not established. Since water molecules are being oriented in more favourable way by this step, a great amount of potential energy is removed. This large amount of potential energy would be converted into a kinetic energy during the MD, which might disrupt chosen temperature regime of MD simulation. Atoms in intralayer are frozen in order to keep all structural elements of intralayer intact while water molecules with calcium ions are being optimized according to the structure of intralayer. This geometry relaxation was followed by 5 ps MD simulation with timestep of 0.1 fs under pressure of 1 bar. In this step atoms in the intralayer are also kept frozen, while water molecules and calcium ions are allowed to move. Ensemble of velocities of these atoms are initialized as random numbers and are scaled to be consistent with movements of atoms at 0.1 K. Nose-Hoover thermostat and barostat were used in order to keep temperature of the atoms in intralayer ramping from 0.1 K at the beginning of the simulation up to the 500 K. Pressure was kept constant at 1 bar. Since the large part of the unit cell is frozen, the temperature is not defined quantity in this case, but the amount of kinetic energy on atoms in the interlayer is more than enough to enable atoms moving from the energy minimum set by the geometry optimization. Following steps: geometry optimization without frozen atoms, low temperature MD and finally unconstrained geometry optimization are used in order to relax structure prior the long MD steps. The next MD step is the simulation of heating of the system to 300 K over 5 ps period. This step is used in order to give atoms enough energy to surpass energy barriers of initial energy minimum in order to settle it to some, possibly lower minimum in the following step. Timestep for integration of equations of motions in this MD step is 0.5 fs and initial atomic velocities are chosen as random numbers and scaled to correspond to atomic velocities at 0.1 K. Geometries obtained from the relaxation step (calculation step 5), and the MD step (calculation step 7) are re-optimized with the $\text{ReaxFF}_{\text{SiO:CaO}}$ parameter set, without disabled O–H bonding.

The procedure we used for optimization of crystal structure of C–S–H allows the movement of water molecules and Ca ions. However, the Si–O skeleton remains, ant thus it is not possible to obtain a structure from 'another model' during the optimization. Such transformation (between different models) would require passing through energetic barriers which are by order of magnitude larger than the energy applied to the system during MD simulations.

In addition, geometries, optimized with ReaxFF, are reoptimized with the PM6 semiempirical method [26] implemented into a MOPAC program package. The

semiempirical calculations are performed in order to verify results with quantum chemical calculations.

3 Results ans discussion

3.1 Structures

After the geometry optimization and molecular dynamics calculations, in final geometries the layered structure of C–S–H particles is conserved. Majority of water molecules are still contained within the interlayer, however in models 2 and 3 some water molecules and OH^- diffused into the intralayer.

Since the computational procedure we used for building models 1, 2 and 3 was tailored to set optimal positions of water molecules, resulting geometries can provide information about the distribution of water inside these models. During the calculation step 2 in which molecular dynamics technique is used to diffuse water molecules through the space between silica skeleton, water molecules as expected filled all available space, left from the box-constrained minimization. Since the space between silica groups is limited, the distribution of water molecules is not random. During the simulation water molecules and OH^- groups moved and diffused from interlayer to voids created during the removal of Si atoms.

Since all models agree on several key observations: rows of silica oligomers, flanked by rows of water molecules from each side and also these doubled layers flanked by thin layers of water molecules from the top and the bottom, the general structure of C–S–H can be established.

Geometries obtained with semiempirical calculations produce the similar geometrical features as the calculations with ReaxFF force field. The Si–O bond lengths are more uniform in PM6 geometries. Parametrization used in $ReaxFF_{SiO:CaO}$ has a tendency to assign partial covalent character to interactions between oxygen and calcium atoms. If the oxygen atom from a non-bridging Si–O bond is near calcium atom, it's bond might weaken since it is involved in partial bond with a calcium atom. Calculations with PM6 hamiltonian, especially with non optimal initial geometry, might converge to a structure with too short interatomic distance between oxygen atoms. These bonds are usually created between Si–O and OH^- group or between geminal oxygen Si–O atoms (resulting in SiO_2 ring). In our study we rejected the structures with such non-physical geometry. It is fair to conclude that re-optimization of stable geometries with PM6 hamiltonian leads to minor changes in interatomic distances and the main change (in compar-

Table 4: Heat of formation (eV) for most stable structures within different models of C–S–H per unit cell. MIN – minimal value, MED – median value, IQR – interquartile range.

H/S ratio		ReaxFF			PM6		
		Model 1	Model 2	Model 3	Model 1	Model 2	Model 3
1.4	MIN	−2605.97	−2588.2	−2562.68	−2491.68	−2480.18	−2464.69
	MED	−2594.22	−2573.44	−2553.46	−2484.18	−2468.7	−2457.63
	IQR	8.61	14.35	9.42	7.93	16.47	12.97
1.6	MIN	−2675.55	−2664.41	−2642.68	−2541.39	−2527.5	−2526.27
	MED	−2665.93	−2655.78	−2630.36	−2537.17	−2518.93	−2512.31
	IQR	2.2	5.42	14.5	3.76	15.72	6.75
1.8	MIN	−2746.39	−2746.14	−2721.61	−2593.46	−2579.63	−2575.3
	MED	−2737.31	−2733.56	−2711.47	−2588.61	−2570.39	−2566.93
	IQR	7.82	9.46	22.96	4.28	2.65	11.93
2.0	MIN	−2813.12	−2822.13	−2807.62	−2648.7	−2638.89	−2628.98
	MED	−2807.86	−2812.44	−2786.29	−2641.77	−2624.85	−2620.67
	IQR	6.28	11.64	13.2	3.74	11.8	15.31

ison to ReaxFF) is related to better description of electronic distribution and thus, to more reliable description of the total energy.

3.2 Energies

Calculated energies can be used for the comparison of stability of C–S–H structures, presented by different models. In contrary to previously suggested in [15] structures, models 1, 2 and 3 have the identical composition, and thus the energies can be compared directly and without any additional assumptions. In all structures, the kinetic energy has a minor contribution in the enthalpy ($\approx 0.6\%$) at 300 K. The low contribution of the kinetic energy is a consequence of tightly bound molecules and ions. Since all MD calculations were done in the constant pressure environment, PV component of enthalpy is constant and can be neglected in energy comparisons.

The heat of formation for the structures in a particular model (the minimal value for each set of structures, the median value, and the interquartile range) are presented in Table 4 . Although the absolute values of the heat of formation are large, one should not forget that they were computed for unit cells containing from 1075 to 1258 atoms.

The values of heat of formation computed for different structures in models 1-2-3 are not completely separated in energy scale. Some structures from model 1

Table 5: The densities of models 1, 2, 3 with different H/S ratios. Densities (g/cm^3) are calculated on geometries after MD calculation with ReaxFF force field and after geometry optimization at PM6 theory. The deviation of densities of individual structures inside a model is below $0.02\ g/cm^3$.

H/S ratio	ReaxFF			PM6		
	Model 1	Model 2	Model 3	Model 1	Model 2	Model 3
1.4	2.56	2.26	2.23	2.68	2.52	2.47
1.6	2.53	2.26	2.22	2.67	2.5	2.46
1.8	2.49	2.27	2.22	2.64	2.5	2.47
2.0	2.40	2.27	2.21	2.62	2.48	2.45

show the lowest heat of formation and thus, they are energetically more stable. In the same time, some other structures from the same model have higher energies than structures with lowest energies from models 2 and 3. However, the majority of the structures from model 1 have lower energies, as proved by median value of heat of formation. The spread of the values of energies inside the same model and the same chemical composition (presented as interquartile range) is (in most of the cases) small in comparison to the difference between median values for different models.

The difference in heat of formation for the structures from different models optimized with ReaxFF Hamiltonian is less pronounced. For the structures with low content of water: model 1 is most stable, followed by 2 and 3. With increase of water content, the difference between model 1 and 2 becomes smaller, and for large H/S ratio model 2 structures have slightly lower energies.

Quantum chemical semiempirical methods use information about distribution of electrons and thus they provide more reliable and less sensitive (with respect to the selection of parameters) description of molecules and crystals. The results obtained with PM6 Hamiltonian give a preference for model 1 for all H/S ratio.

3.3 Density

The densities of models 1, 2 and 3 (see Table 5) are systematically larger than densities of the corresponding models ($1^{\dagger}$–$3^{\dagger}$) presented earlier in [15]. That difference can be attributed to the difference in methods of construction of models: In models 1, 2 and 3 the positions of water molecules are allowed to diffuse through the structure and fill all available cavities, while in models $1^{\dagger}$–$3^{\dagger}$, water molecules are deduced from the corresponding crystallographic sites in tobermorite and their

Table 6: Average bonding parameters in structures created according to models 1–3. In paranthesis the values are calculated from Si–O–Si connectivity and Ca coordination, according [30].

	ReaxFF			PM6		
	Model 1	Model 2	Model 3	Model 1	Model 2	Model 3
Average Si–O–Si connectivity	1.18	1.18	1.09	1.18	1.29	1.09
Average Si–O bond length, Å	1.55 (1.63)	1.55 (1.63)	1.55 (1.63)	1.64 (1.63)	1.64 (1.63)	1.64 (1.63)
Average Ca coordination number	6.86	6.55	6.46	6.27	5.99	5.93
Average volume of Ca coordination polyheda, $Å^3$	23.09 (20.88)	21.93 (19.61)	21.42 (19.24)	16.88 (20.88)	15.10 (19.61)	14.78 (19.24)
Average Ca–O bond length, Å	2.56 (2.43)	2.54 (2.43)	2.54 (2.43)	2.39 (2.43)	2.37 (2.43)	2.37 (2.43)

positions are only modified by the relaxation procedure that optimized geometry and unit cell size to the nearest energy minimum. Within presented models, only model 1 shows the change in density with respect to the H/S ratio. The change in density is caused by thickening of water layers as H/S ratio is increased. The same trend is not observed in models 2 and 3.

That trend follows experimentally measured trend [27]. Also, model 1 shows the density closest to the experimental one [28, 29]. The lower density, as predicted by $ReaxFF_{SiO:CaO}$ force field, is a consequence of longer Si–O bonds and longer hydrogen bonds.

In Table 6 we present the analysis of average bonding parameters for models 1–3 and compare the data with one suggested by I. G. Richardson [30]. The average distances between Si–O and Ca–O computed by semiempirical PM6 Hamiltonian matching the experimental data. However the difference between models itself is too small and can not be used as an extra argument in favour of one or another model. The detailed information about the distribution of structural parameters in models 1–3 is given in the supplementary data.

4 Conclusions

New models for the structure of the C–S–H are proposed. A set of different structures that belong to these models are relaxed by geometry optimizations and molecular dynamics simulations. After geometry optimization and molecular dynamics calculations, water molecules organized into a two different structural features: rows and sheets. Rows of water molecules are positioned between the rows of silica units. Energetically the most stable model is model 1. The same model have the largest density, which corresponds to the experimentally observed values. Unlike models 2 and 3, the density of model 1 changes with respect to the H/S ratio and the change follows experimentally observed trend. The knowledge about the atomic structure of bulk C–S–H will simplify the future study of stability of C–S–H surfaces, interfaces to water and formation of finite size C–S–H particles.

Acknowledgement: This research was financed by the BASF Construction Solutions. The calculations were performed on resources provided by the Swedish National Infrastructure for Computing (SNIC) at LUNARC.

References

1. H. F. W. Taylor, *Cement Chemistry*, 2nd edn., Thomas Telford Publishing, London (1997).
2. S. Garrault, E. Lesniewska, and A. Nonat, Mater. Struct. **38** (2005) 435.
3. T. Powers, J. Am. Ceram. Soc. **41** (1958) 1.
4. A. Nonat, Cement Concrete Res. **34** (2004) 1521.
5. X. Cong and R. Kirkpatrick, Adv. Cem. Based Mater **3** (1996) 144.
6. I. G. Richardson, Cement Concrete Res. **9** (2004) 1733.
7. G. Renaudin, J. Russias, F. Leroux, F. Frizon, and C. Cau-Dit-Coumes , J. Solid State Chem. **182** (2009) 3312.
8. S. A. Hamid, Z. Kristallogr. **154** (1981) 189.
9. K. Garbev, G. Beuchle, M. Bornefeld, L. Black, and P. Stemmermann, J. Am. Ceram. Soc. **91** (2008) 3005.
10. J. Chen, J. Thomas, H. F. W. Taylor, and H. Jennings, Cement Concrete Res. **34** (2004) 1499.
11. R. J.-M. Pellenq, A. Kushima, R. Shahsavari, K. J. V. Vliet, M. J. Buehler, S. Yip, and F.-J. Ulm, P. Natl. Acad. Sci. USA **106** (2009) 16102.
12. M. J. Abdolhosseini Qomi, K. J. Krakowiak, M. Bauchy, K. L. Stewart, R. Shahsavari, D. Jagannathan, D. B. Brommer, A. Baronnet, M. J. Buehler, S. Yip, F.-J Ulm, K. J. Van Vliet, and R.J-.M. Pellenq, Nat. Commun. **5** (2014) Art. 4969.
13. A. Nonat and X. Lecoq, TS[c], in: *Nuclear Magnetic Resonance Spectroscopy of Cement Based Materials*, A. G. P. Colombet, H. Zanni, P. Sozzani (Eds.) Spinger, Berlin (1998), p. 197–207.

TS[c] Please add the title of the chapter.

Editor's or typesetter's annotations (will be removed before the final TEX run)

14. B. Lothenbach and A. Nonat, Cement Concrete Res. **78** (2015) 57.
15. G. Kovačević, B. Persson, L. Nicoleau, A. Nonat, and V. Veryazov, Cement Concrete Res. **67** (2015) 197.
16. S. Merlino, E. Bonaccorsi, and T. Armbruster, Eur. J. Mineral., **13** (2001) 577.
17. H. Manzano, S. Moeini, F. Marinelli, A. C. Van Duin, F. J. Ulm, and R. J. M. Pellenq, J. Am. Chem. Soc. **134** (2012) 2208.
18. D. Hou, T. Zhao, H. Ma, and Z. Li, J. Phys. Chem. C **119** (2015) 1346.
19. C. Labbez, I. Pochard, B. Jönsson, and A. Nonat, Cement Concrete Res. **42** (2011) 161.
20. L. Martínez, R. Andrade, E. G. Birgin, and J. M. Martínez, J. Comput. Chem. **30** (2009) 2157.
21. J. M. Martínez and L. Martínez, J. Comput. Chem. **24** (2003) 819.
22. S. Plimpton, J. Comput. Phys. **117** (1995) 1.
23. A. C. van Duin , S. Alejandro, S. Shannon, Z. Qingsong, X. Xin, and W. A. Goddard III, J. Phys. Chem. A **107** (2003) 3803.
24. H. Manzano, E. Masoero, I. Lopez-Arbeloa, and H. M. Jennings, Soft Matter **9** (2013) 7333.
25. H. Manzano, R. J. M. Pellenq, F.-J. Ulm, M. J. Buehler, and A. C. van Duin, Langmuir **28** (2012) 4187.
26. J. J. P. Stewart, J. Mol. Model. **13** (2007) 1173.
27. J. J. Thomas, H. M. Jennings, and A. J. Allen, J. Phys. Chem. C **114** (2010) 7594.
28. A. J. Allen, J. J. Thomas, and H. M. Jennings, Nat. Mater. **6** (2007) 311.
29. A. C. A. Muller, K. L. Scrivener, A. M. Gajewicz, and P. J. McDonald, J. Phys. Chem. **117** (2013) 403.
30. I. G. Richardson, Acta Cryst. B **69** (2013) 150.

Supplementary material: The online version of this article
(DOI: 10.1515/zpch-2015-0718) provides supplementary material for authorized users.